



## Research Article

<https://doi.org/10.1631/jzus.A2500581>

# Evaluating and predicting tunnel overbreak by integrating cloud modeling and fuzzy evaluation theory

Shibin YAO<sup>1</sup>, Jian ZHOU<sup>1</sup>✉, Biao HE<sup>2</sup>, Chuanqi LI<sup>1</sup>✉

<sup>1</sup>School of Resources and Safety Engineering, Central South University, Changsha 410083, China

<sup>2</sup>Civil, Structural & Environmental Engineering, University College Cork, Cork, Ireland

**Abstract:** Tunnel overbreak is a common but unfavorable phenomenon in drill-and-blast excavation, leading to increased construction costs, delayed schedules, and potential stability risks. Accurate evaluation and prediction of overbreak are therefore important for tunnel construction control. In this paper, we propose a cloud-model-based comprehensive evaluation and prediction framework developed by integrating fuzzy evaluation theory with subjective and objective weighting methods. A dataset containing 523 records from the HuXiTai (HXT) tunnel was used, and seven routinely obtainable geological and blasting indicators were selected to construct the evaluation system. Eight weighting strategies were compared, including conventional objective methods, expert judgment, and a ridge-regression-based objective method. The best-performing objective weights were further combined with subjective weights to establish the final comprehensive evaluation model. The results show that the proposed model achieved an overbreak evaluation accuracy of 85.28%. In addition, the comprehensive evaluation score showed a strong linear relationship with the measured overbreak area, yielding a prediction  $R^2$  of 0.85. The cloud model representation further enabled intuitive visualization of overbreak risk levels and transitional characteristics between adjacent grades. Overall, the proposed framework provides a practical and interpretable tool for overbreak risk evaluation and quantitative prediction in tunnel blasting construction.

**Key words:** Tunnel overbreak; Risk assessment; Cloud model; Fuzzy theory; Ridge regression

## 1 Introduction

The drill-and-blast method remains one of the most widely used excavation techniques in tunnel and underground engineering because of its flexibility, efficiency, and economic applicability. With the increasing scale and complexity of tunnel construction, higher requirements have been placed on excavation quality, construction safety, and overbreak control (Dong et al., 2022; Liu et al., 2024; Zhang et al., 2024). During drill-and-blast excavation, unfavorable geological conditions, unreasonable blasting design, and construction deviations may

cause the actual tunnel contour to exceed the designed profile, a phenomenon known as overbreak (Fig. 1). Overbreak can increase excavation and support costs, delay construction progress, and locally weaken the surrounding rock, thereby affecting structural stability and construction safety (Verma et al., 2018; Liu et al., 2024). Therefore, accurate evaluation and prediction of overbreak are important for optimizing blasting design, identifying high-risk excavation sections, and supporting timely control measures during tunnel construction.

Previous studies have examined tunnel overbreak from the perspectives of geological conditions, drilling accuracy, rock mass quality, and blasting parameters. Mandal and Singh (2009) evaluated the extent and causes of tunnel overbreak, while Foderà et al. (2020) analyzed the factors influencing overbreak volumes in drill-and-blast tunnel excavation. Gong et al. (2026a) provided experimental evidence on fracture behavior and fracture-surface morphology, which is helpful for

✉ Jian ZHOU, j.zhou@csu.edu.cn

Chuanqi LI, chuanqi.li@csu.edu.cn

Jian ZHOU, <https://orcid.org/0000-0003-4769-4487>

Chuanqi LI, <https://orcid.org/0000-0002-8163-5432>

Received Nov. 13, 2025; Revision accepted May 2, 2026;  
Crosschecked

understanding rock damage characteristics related to excavation response. Barton (2002) provided Q-system-related correlations for site characterization and tunnel design, and Ganesan and Mishra (2021) emphasized drilling inaccuracy and the distinction between constructional and geological overbreak. Dey and Murthy (2012) developed a method for predicting blast-induced overbreak under uncontrolled burn-cut blasting conditions, and Torres et al. (2023) presented a post-work inspection method for overbreak assessment. Field-based studies suggested that improved drilling accuracy, optimized charge placement, and refined contour control can reduce overbreak (Kim and Moon, 2013; Lee et al., 2016). These studies provided an important engineering understanding of overbreak formation and control. However, many empirical, experimental, or field-based approaches remain closely linked to specific geological conditions, rock damage characteristics, and construction practices, which limits their direct use in a unified and interpretable evaluation framework.

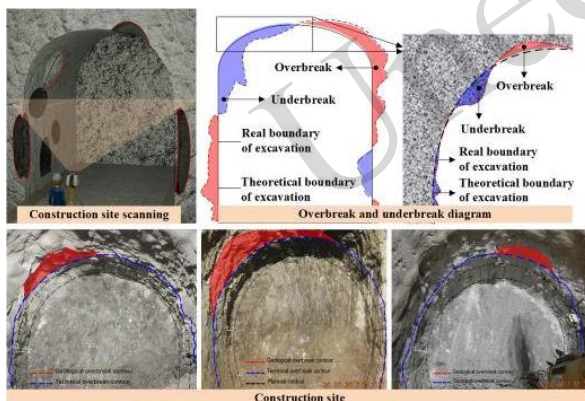


**Fig. 1** Schematic diagram of tunnel overbreak and scanning (construction site image adapted from Foderà et al., 2020).

With the development of numerical simulation, experimental testing, and three-dimensional modeling techniques, simulation-based and experimental–numerical approaches have been increasingly used to analyze blast-induced damage and overbreak evolution (Gong et al., 2026b). Daraei and Zare (2018) predicted overbreak depth using strength factors, while Hong et al. (2023a) combined experimental and numerical methods to investigate blast-induced overbreak and underbreak in underground roadways. Chen et al. (2021b) investigated overbreak control considering the

influence of initial support, Li et al. (2023) analyzed the influence of key blasthole parameters on tunnel overbreak, and Hong et al. (2023c) examined the overbreak and underbreak behavior of pre-stressed tunnels under decoupled charge blasting. These studies have improved the mechanistic understanding of tunnel overbreak, but numerical models generally require detailed parameter calibration and are often case-specific, which may limit their direct use for rapid overbreak risk evaluation during routine construction.

With the development of intelligent computing, machine learning and soft-computing methods have been increasingly applied to tunnel overbreak prediction. Jang and Topal (2013), Sun et al. (2013), and Mottahedi et al. (2018) used regression models, neural networks, fuzzy logic, ANFIS, and support vector machines to predict overbreak under different geological and blasting conditions. Jang et al. (2019), Koopialipour et al. (2019), and Jang (2020) further improved overbreak analysis by introducing the overbreak resistance factor, optimization algorithms, and tunnel overbreak management systems. More recently, ensemble learning, metaheuristic optimization, Bayesian optimization, data augmentation, and gene expression programming have been introduced to enhance prediction performance and model applicability (Torres et al., 2023; Liu et al., 2023; Hong et al., 2023b; Im et al., 2025; Taheri et al., 2025). These studies have demonstrated the potential of intelligent models for nonlinear overbreak prediction, but many still emphasize prediction accuracy rather than risk-grade evaluation, uncertainty representation, and interpretable engineering decision support.

Similar data-driven approaches have also been widely used in blasting-response and geotechnical prediction studies. Zhou et al. (2020) and Zeng et al. (2021) developed intelligent models for blast-induced vibration prediction, while Zhao et al. (2022) and Ghani et al. (2024) showed that hybrid optimization and ensemble learning can improve nonlinear mapping and prediction robustness in complex engineering problems. These studies, together with recent reviews on tunnel blasting and overbreak control, indicate that data-driven models can provide useful support for construction safety and quality control (He et al., 2024a; Verma et al., 2018).

Nevertheless, the multifactorial nature of overbreak, together with limitations in data quantity, quality, and diversity, still restrict the broader applicability of purely prediction-oriented models.

To address these limitations, we propose a cloud-model-based comprehensive evaluation and prediction framework for tunnel overbreak by integrating fuzzy evaluation theory with subjective and objective weighting methods. Unlike studies that focus mainly on direct numerical prediction, the proposed framework aims to combine qualitative risk grading, uncertainty representation, and quantitative overbreak area (OB) prediction within a unified model. This idea is consistent with recent engineering prediction studies emphasizing transparent, interpretable, and practically usable data-driven frameworks (Benzaamia et al., 2024, 2025). A dataset containing 523 records collected from the HuXiTai (HXT) tunnel was used, and seven routinely obtainable geological and blasting indicators were selected to construct the evaluation system, including rock mass rating (RMR), cross-sectional area (CSA), charge depth ratio (CDR), powder factor (PF), advance length (AL), hole density (HD), and drill hole depth (DH). Multiple weighting methods were compared, and a ridge-regression-based objective weighting method was combined with expert

judgment to establish the final comprehensive evaluation model. Cloud modeling was then used to visualize overbreak risk grades and their transitional characteristics, while the comprehensive evaluation score was further used for quantitative OB prediction.

The remainder of this paper is organized as follows: Section 2 introduces the dataset and evaluation indicators; Section 3 presents the proposed methodology; Section 4 discusses the overbreak risk evaluation results; Section 5 presents the quantitative prediction of overbreak area; and Section 6 summarizes the main conclusions.

## 2 Data collection and analysis

### 2.1 Data sources

The dataset used in this study was collected from the HuXiTai (HXT) tunnel during drill-and-blast excavation (He et al., 2023, 2024b). The HXT tunnel is a twin-bore highway tunnel located in Tonglu County, Hangzhou, China, connecting Yao Lin Town and Hengcun Town (Fig. 2). The right and left tunnel lines are 3125 m and 3122 m long, respectively. The surrounding strata consist mainly of Quaternary residual slope deposits, quartzite interbedded with muddy sandstone, muddy sandstone interbedded with quartzite, and limestone.

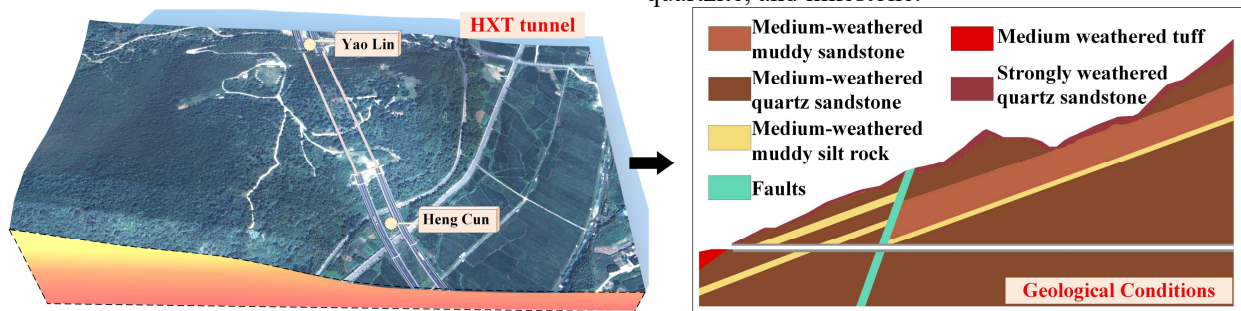


Fig. 2 Topographical and geological settings along the HXT tunnel alignment.

A total of 523 excavation records were used for overbreak evaluation and prediction. The dataset includes both geological and blasting-related information, with the OB taken as the target variable. Based on literature review, expert consultation, and data availability, seven routinely obtainable indicators were selected as model inputs: rock mass rating (RMR), cross-sectional area (CSA), charge depth ratio (CDR), powder factor (PF), advance length (AL), hole density (HD), and drill hole depth (DH). RMR

was included to represent the combined influence of rock strength, rock quality designation, discontinuity spacing, discontinuity condition, groundwater condition, and discontinuity orientation. These indicators provide the basis for constructing the subsequent overbreak evaluation and prediction model.

### 2.2 Data characteristics and correlation analysis

The seven input indicators, namely RMR, CSA, CDR, PF, AL, HD, and DH, were collected from the

HXT tunnel dataset, with OB used as the output indicator. The distributions of the 523 records are shown in Fig. S1 of the Electronic Supplementary Materials. Although the values of each indicator are concentrated within certain ranges, dispersion is still evident, reflecting the variability of geological conditions and blasting parameters during tunnel excavation.

To examine the relationships between the input indicators and OB, a correlation analysis was conducted (Fig. 3). CSA showed a negative correlation with OB, whereas the other indicators showed positive correlations. CDR had the strongest correlation with OB, with a correlation coefficient of 0.91. From a purely machine-learning perspective, highly correlated indicators may sometimes be removed to reduce redundancy. However, in the fuzzy evaluation framework adopted in this study, such indicators can provide representative information for risk grading and are therefore retained. The other indicators also showed relatively strong correlations with OB, with correlation coefficients greater than 0.55, supporting their use in the overbreak evaluation system.

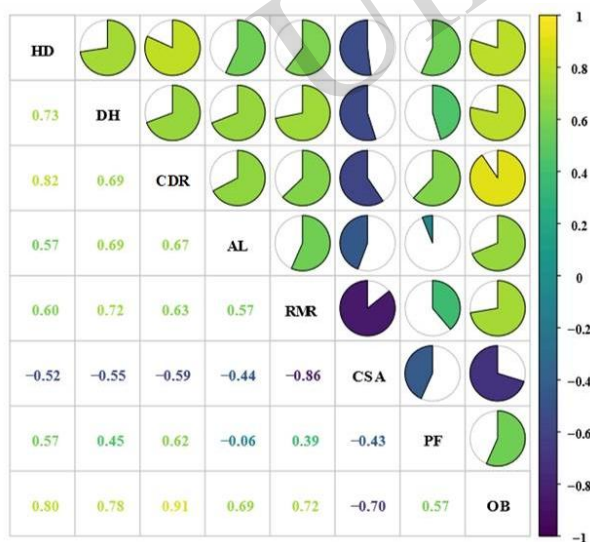


Fig. 3 Data correlation analysis chart.

Overall, the dataset exhibited clear heterogeneity among the geological and blasting indicators, indicating that overbreak is influenced by multiple interacting factors rather than by a single dominant variable. Similar data-driven studies have also emphasized that predictive performance should be

interpreted together with the data source, parameter coverage, and testing strategy (Zhou et al., 2020; Sarir et al., 2021). Note that the 523 records used in this study were collected from one tunnel project. Therefore, the dataset supports within-project evaluation and prediction, while the transferability of the proposed framework should be further validated using multi-project datasets under different geological and construction conditions.

### 3 Fuzzy integrated evaluation based on cloud modeling

Fuzzy evaluation theory has been widely used in multi-indicator engineering risk assessment because it can describe qualitative grades under uncertain boundaries (Gong et al., 2022; Zhou et al., 2022b). In this study, fuzzy evaluation theory was combined with cloud modeling to establish an overbreak evaluation and prediction framework. The overall procedure includes indicator grading, weight determination, comprehensive evaluation, cloud-model visualization, and OB prediction.

#### 3.1 Grading of evaluation indicators

The seven input indicators, namely RMR, CSA, CDR, PF, AL, HD, and DH, together with the output indicator OB, were graded according to the evaluation criteria adopted from previous studies and the distribution characteristics of the HXT tunnel dataset (Li and Wu, 2019). The value range of each indicator was mapped onto a corresponding score interval, and the overbreak risk was divided into five levels: Level 1, low risk; Level 2, low-medium risk; Level 3, medium risk; Level 4, medium-high risk; and Level 5, high risk. The evaluation indicators and grading criteria are shown in Fig. 4.

The complete evaluation and prediction process is shown in Fig. 5. First, the original geological and blasting indicators were graded according to the established criteria. Second, multiple weighting methods were used to determine the relative importance of the indicators. Third, the comprehensive evaluation score was calculated by integrating the graded indicators and their weights. Finally, cloud modeling was used to visualize the overbreak risk level, and the comprehensive evaluation score was further used for quantitative OB

prediction.

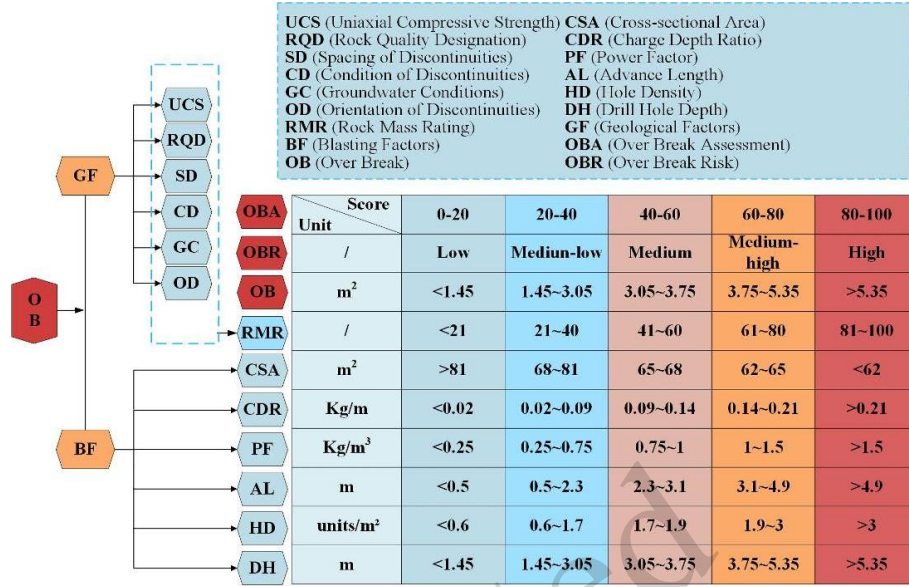


Fig. 4 Evaluation indicators and criteria.

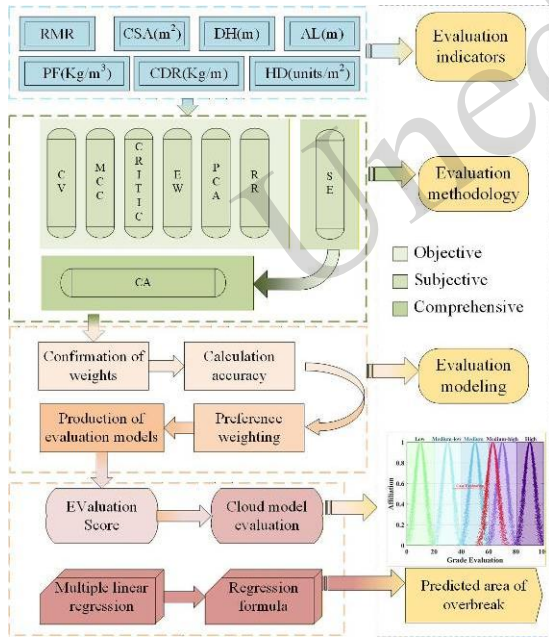


Fig. 5 Complete evaluation and prediction flowchart for overbreak.

### 3.2 Weight determination and comprehensive evaluation

To determine the relative importance of different evaluation indicators, both objective and subjective weighting methods were considered. Suppose that there are  $m$  evaluation indicators and  $n$  evaluation objects. The original evaluation matrix can be expressed as:

$$\begin{bmatrix} x_{11} & x_{12} & \cdots & x_{1m} \\ x_{21} & x_{22} & \cdots & x_{2m} \\ \vdots & \vdots & \ddots & \vdots \\ x_{n1} & x_{n2} & \cdots & x_{nm} \end{bmatrix} \quad (1)$$

where  $x_{ij}$  represents the  $j$ -th indicator for the  $i$ -th evaluation object.

Five conventional objective weighting methods were first adopted as comparative strategies: the coefficient of variation (CV) method, which reflects the relative dispersion of each indicator (Zhao and Zhong, 2009); the multi-correlation coefficient (MCC) method, which evaluates the independent information contained in each indicator (Xiao et al., 2023); the criteria importance through intercriteria correlation (CRITIC) method, which considers both contrast intensity and conflict among indicators (Krishnan et al., 2021; Chen et al., 2021a); the entropy weight (EW) method, which determines weights according to information entropy (Liang et al., 2019; Zhou et al., 2022a, 2022c, 2022d); and the principal component analysis (PCA) method, which transforms correlated indicators into uncorrelated principal components while retaining the main information of the original dataset (Bi et al., 2021; Lei et al., 2022). These methods represent different data-driven weighting perspectives, including dispersion, redundancy, information content, and dimensionality reduction.

Their detailed formulations are provided in Section S2 of the Electronic Supplementary Materials.

To improve the objectivity and stability of the weighting process, a ridge-regression-based weighting method (RR), which combines linear regression with coefficient regularization, was further introduced in this study (Friedman et al., 2010). Since the evaluation indicators have different numerical scales, all input indicators were first standardized using z-score normalization (Asteris et al., 2020):

$$z_{ij} = \frac{x_{ij} - \mu_j}{\sigma_j} \quad (2)$$

Ridge regression was then performed using the standardized indicators as input variables and the measured OB as the output variable. The regression model and its objective function can be expressed as:

$$\hat{y}_i = \beta_0 + \sum_{j=1}^m \beta_j z_{ij} \quad (3)$$

$$L = \sum_{i=1}^n (y_i - \hat{y}_i)^2 + \alpha \sum_{j=1}^m \beta_j^2 \quad (4)$$

After model fitting, the absolute values of the standardized regression coefficients were normalized to derive the final objective indicator weights:

$$w_j = \frac{|\beta_j|}{\sum_{j=1}^m |\beta_j|} \quad (5)$$

where  $x_{ij}$  is the original value of the  $j$ -th indicator for the  $i$ -th sample;  $\mu_j$  and  $\sigma_j$  are the mean and standard

deviation of the  $j$ -th indicator, respectively;  $\hat{y}_i$  is the predicted OB;  $\beta_0$  is the intercept term;  $\beta_j$  is the standardized regression coefficient of the  $j$ -th indicator;  $z_{ij}$  is the standardized value of the  $j$ -th indicator;  $y_i$  and  $\hat{y}_i$  are the actual and predicted OBs of the  $i$ -th sample, respectively;  $\alpha$  is the regularization parameter selected by five-fold cross-validation;  $m$  is the total number of indicators.  $w_j$  is the normalized weight assigned to the  $j$ -th indicator.

As shown in Fig. 6, different candidate  $\alpha$  values were evaluated using multiple metrics, including  $R^2$ , RMSE, MAE, and a20, where  $R^2$  was used to reflect the explanatory capability of the fitted model (Nakagawa and Schielzeth, 2013). The optimal  $\alpha$  was 0.3144, under which the RR model achieved an  $R^2$  of 0.8925, RMSE of 0.4982, MAE of 0.3844, and a20 of 0.8279. These metrics were used following common practice in machine-learning-based engineering prediction studies (Le et al., 2022; Asteris et al., 2024). The use of ridge regularization and cross-validation also helps reduce the risk of overfitting and improve the stability of the weighting process, which is consistent with previous machine-learning-based engineering prediction studies (Armaghani and Asteris, 2021; Asteris et al., 2021).

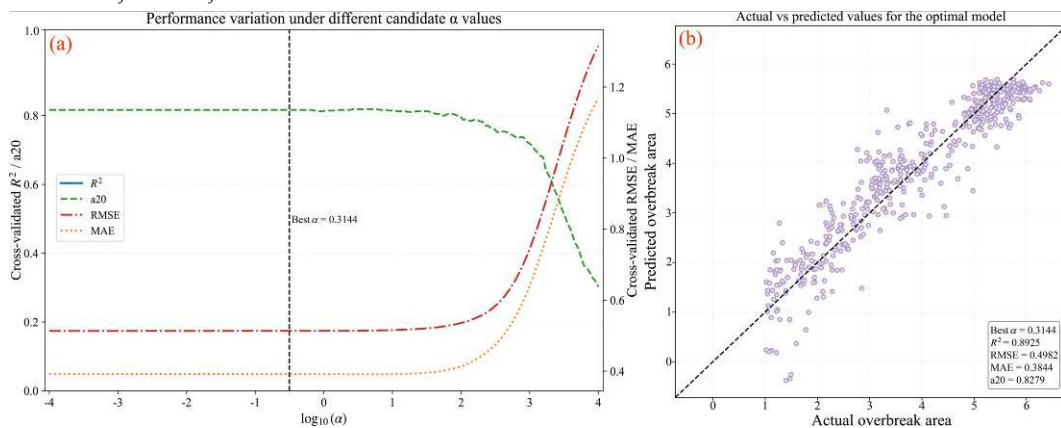


**Fig. 6** Optimization and fitting performance of the ridge-regression-based weighting method: (a) variation of cross-validated  $R^2$ , RMSE, MAE, and a20 under different candidate  $\alpha$  values; and (b) actual-versus-predicted comparison for the optimal model.

In addition to objective weighting, expert judgment was used to provide subjective weights based on engineering knowledge. This is necessary

because overbreak is controlled by multiple interacting geological and blasting factors, and some engineering mechanisms may not be fully captured by

data-driven weighting alone (Yang et al., 2024). A panel consisting of one frontline technical expert, two industry professors, and two researchers independently assigned weights to the seven indicators, and the final subjective weights were obtained by averaging their results. Further details of the subjective weighting procedure are provided in the Electronic Supplementary Materials (Section S2.6).

The final comprehensive evaluation (CE) weights were obtained by combining the best-performing objective weights with the subjective weights. This combined weighting strategy follows the idea that subjective knowledge and objective data information can complement each other in multi-indicator engineering evaluation (Zhao et al., 2021; Chen et al., 2025; Yao et al., 2025a). The combined weight of each indicator can be expressed as:

$$w_j^{CE} = \frac{w_j^{obj} + w_j^{sub}}{2} \quad (6)$$

where  $w_j^{CE}$ ,  $w_j^{obj}$ , and  $w_j^{sub}$  are the combined, objective, and subjective weights of the  $j$ -th indicator, respectively.

Based on the obtained combined weights, the comprehensive evaluation score of the  $i$ -th sample was calculated as:

$$S_i = \sum_{j=1}^m w_j^{CE} r_{ij} \quad (7)$$

where  $S_i$  is the comprehensive evaluation score of the  $i$ -th sample,  $r_{ij}$  is the graded score of the  $j$ -th indicator for the  $i$ -th sample, and  $m$  is the total number of indicators.

In this study, the classification accuracy under the overbreak grading criterion was used to compare different weighting strategies and select the most suitable objective weighting method. The classification accuracy is defined as:

$$A = \frac{N_c}{N} \times 100\% \quad (8)$$

where  $A$  is the classification accuracy,  $N_c$  is the number of correctly classified samples, and  $N$  is the total number of samples.

Further details of the CE procedure are provided in the Electronic Supplementary Materials (Section S2.7).

### 3.3 Introduction to cloud modeling theory

Cloud models, which are based on fuzzy mathematics and probability theory, can be classified into forward and inverse cloud models according to the generation path. In this study, the forward normal cloud model was adopted. Specifically, cloud droplets were generated from three numerical characteristics, namely expectation ( $Ex$ ), entropy ( $En$ ), and hyper-entropy ( $He$ ), to describe the randomness and fuzziness of each overbreak risk grade (Fig. 7) (Li et al., 2009). The expectation ( $Ex$ ) was determined as the central value of each evaluation grade interval and serves as the central axis of the cloud model. The entropy ( $En$ ) was calculated based on the width of the corresponding interval to reflect the uncertainty of the qualitative concept and the width of the cloud model. The hyper-entropy ( $He$ ) was set as a small constant proportional to  $En$  to characterize the uncertainty and randomness of entropy, which is reflected by the thickness of the cloud model (Zhou et al., 2026; Yao et al., 2025b).

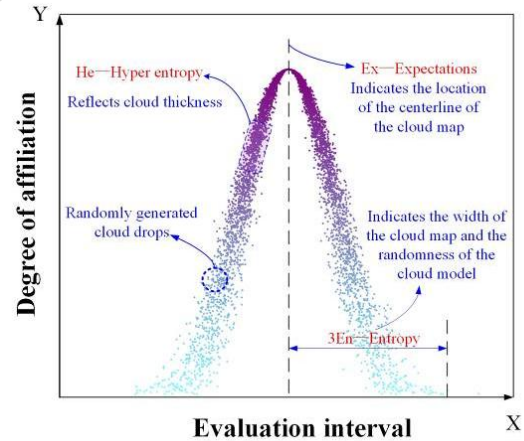


Fig. 7 Schematic diagram of the cloud model.

## 4 Overbreak risk evaluation results based on cloud modeling and fuzzy theory

Based on the established cloud-model-based fuzzy evaluation framework, the 523 excavation records collected from the HXT tunnel were used to conduct overbreak risk evaluation and prediction analysis. In this section, the weighting results obtained from different methods are first compared to identify the most suitable weighting strategy for the HXT tunnel dataset. The evaluation accuracy of each

method is then assessed under the established overbreak grading criterion, based on which the final comprehensive evaluation (CE) model is determined. Subsequently, cloud modeling is used to visualize the overbreak risk level and the transitional characteristics between adjacent grades using both the measured OB values and the CE results. Finally, the relationship between the comprehensive evaluation score and the measured OB is analyzed to verify the applicability of the proposed framework for quantitative overbreak prediction.

#### 4.1 Calculation of weights

The weights obtained by different methods are summarized in Table 1, while the fitting performance of the RR method is shown in Fig. 6. For the RR method, the optimal regularization parameter selected by five-fold cross-validation was 0.3144, under which the model achieved an  $R^2$  of 0.8925, RMSE of 0.4982, MAE of 0.3844, and  $a_{20}$  of 0.8279.

The RR weights ranked as follows: CDR (0.4488), CSA (0.2064), DH (0.1886), RMR (0.0618), AL (0.0443), HD (0.0421), and PF (0.0080). Thus, CDR was identified as the most important indicator, followed by CSA and DH. The final CE weights were obtained by averaging the best-performing objective weights and the subjective weights.

As summarized in Table 1, the weight distributions obtained by different methods showed clear differences. The CV and MCC methods produced relatively less concentrated distributions, although CSA received a noticeably lower weight

than the other indicators. The CRITIC method assigned the largest weight to CSA, while the remaining indicators showed moderate differences. The EW method showed the most concentrated distribution, with more than half of the total weight assigned to CSA. The PCA method also produced an uneven distribution, giving relatively high weights to DH, HD, and AL, but very low weights to CSA and PF. In contrast, the RR, SE, and CE methods showed a more consistent engineering-oriented weighting pattern, in which CDR received the largest weight, while CSA and DH also made important contributions. These differences can also be clearly observed in Fig. 8, which provides an intuitive comparison of the weight distribution characteristics of the seven methods.

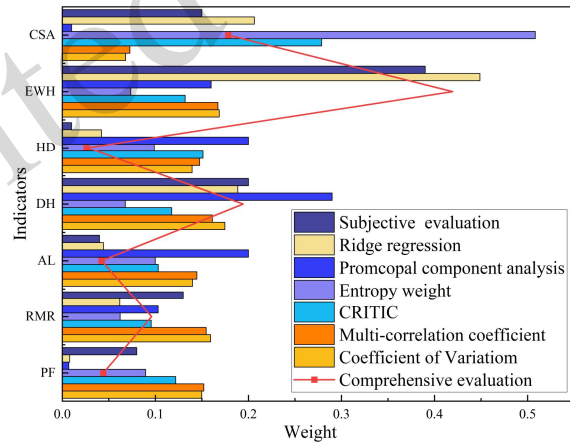


Fig. 8 Comparison of weights obtained by different weighting methods.

Table 1 Weights of evaluation indicators obtained by different weighting methods

Method	Weight						
	CSA	CDR	HD	DH	AL	RMR	PF
CV	0.06810	0.16870	0.13950	0.17470	0.13990	0.15930	0.14990
MCC	0.07270	0.16720	0.14750	0.16120	0.14460	0.15460	0.15210
CRITIC	0.27870	0.13200	0.15120	0.11760	0.10310	0.09550	0.12190
EW	0.50830	0.07360	0.09880	0.06770	0.09990	0.06220	0.08950
PCA	0.01000	0.16000	0.20000	0.29000	0.20000	0.10300	0.00700
RR	0.20640	0.44880	0.04210	0.18860	0.04430	0.06180	0.00800
SE	0.15000	0.39000	0.01000	0.20000	0.04000	0.13000	0.08000
CE	0.17820	0.41940	0.02605	0.19430	0.04215	0.09590	0.04400

#### 4.2 Evaluation accuracy of different weighting methods

Using the weights obtained from the eight weighting methods, the evaluation results of the 523

HXT tunnel records were calculated and compared with the actual overbreak grades. The evaluation accuracy of each method is shown in Fig. 9, and a supplementary comparison is provided in Fig. S4 in

the Electronic Supplementary Materials.

The PCA method produced the lowest evaluation accuracy of 56.21%, while the EW method achieved an accuracy of 67.30%. The CV, MCC, and CRITIC methods showed better applicability, with accuracies ranging from 75% to 79%. Among the objective methods, the RR method achieved the highest accuracy of 83.75%, indicating that the ridge-regression-based weighting strategy can better capture the relationship between the evaluation indicators and overbreak grades. The SE method based on expert judgment achieved an accuracy of 84.70%. After integrating the best-performing objective weights with the subjective weights, the final CE model achieved the highest accuracy of 85.28%.

The CE model was therefore selected as the final overbreak evaluation model. Although some samples were misclassified, most of those were located near adjacent grade boundaries, indicating that the classification errors were generally limited. This result suggests that the combined subjective–objective weighting strategy can improve the stability and applicability of overbreak risk evaluation for the HXT tunnel dataset.

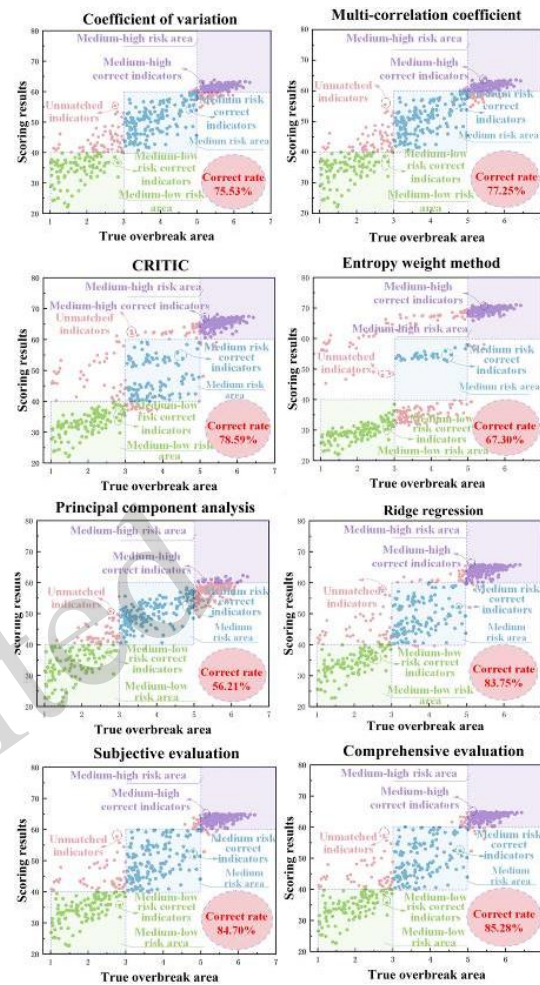


Fig. 9 Data evaluation chart for each theoretical model.

### 4.3 Cloud-model-based overbreak risk evaluation

After establishing the CE model, cloud modeling was used to obtain the overbreak evaluation results and generate cloud maps for overbreak risk assessment.

#### 4.3.1 Integrated evaluation based on cloud model

The overbreak grading standard cloud map was generated according to the grading criteria in Fig. 4. The expectation ( $Ex$ ) was determined based on each grade interval, while  $En$  and  $He$  were set to 4 and 0.6, respectively. A total of 7000 cloud droplets were generated for each grade. The standard cloud map is shown in Fig. 10. The five risk grades correspond to score intervals of 0–20, 20–40, 40–60, 60–80, and 80–100, representing low-risk, low-medium-risk, medium-risk, medium-high-risk, and high-risk levels, respectively.

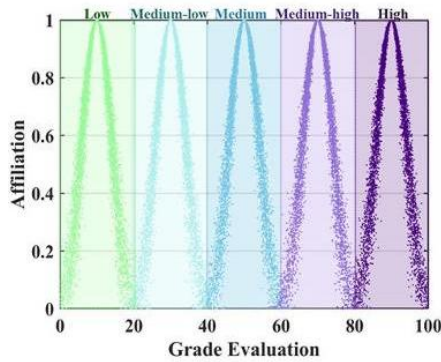


**Fig. 10** Cloud diagram of grading criteria for overbreak evaluation.

To assess the reliability of the subsequent

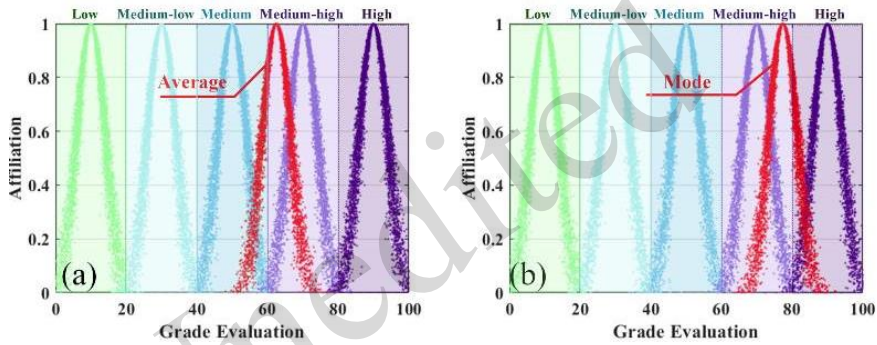


**Fig. 11** Corresponding evaluation cloud diagram of actual overbreak: (a) mean and (b) mode.

### 4.3.2 Comprehensive evaluation of overbreak in HXT tunnel based on cloud modeling

Because the predictive performance of the model has already been evaluated in the previous section, this section focuses on cloud-model-based risk interpretation using representative statistical values, namely the mean and mode, of the indicator dataset.

evaluation, the mean and mode values of the measured OB were calculated and mapped onto the grading standard cloud model. The corresponding results are shown in Fig. 11. As shown in Fig. 11(a), the cloud corresponding to the mean value is distributed mainly in the medium-high-risk interval, although part of the droplet cloud extends toward the adjacent medium-risk range. In Fig. 11(b), the cloud corresponding to the mode shifts further toward the higher-value side while remaining within the medium-high-risk interval. Therefore, both the mean- and mode-based mappings indicate that the actual overbreak condition of the HXT tunnel belongs to the medium-high-risk level.

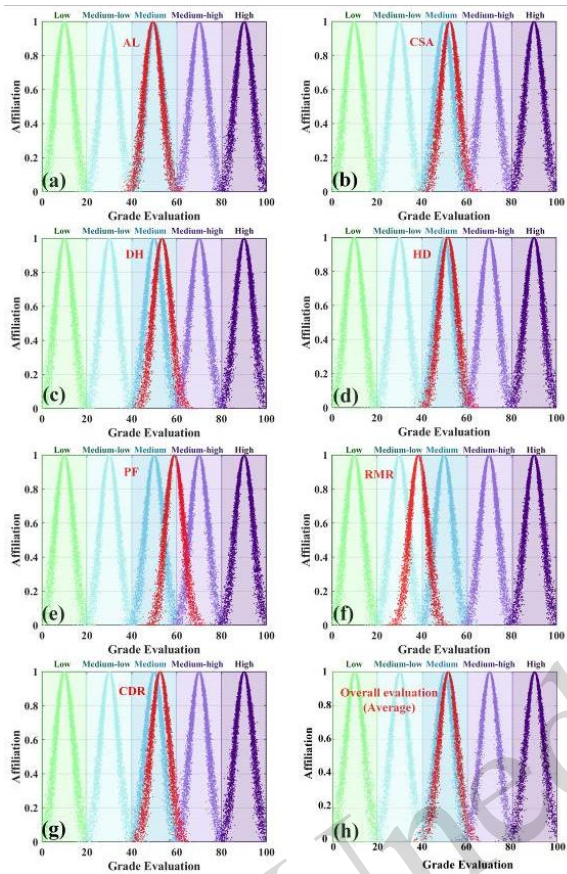


**Fig. 12** CE of overbreak based on cloud modeling using mean values: (a) AL, (b) CSA, (c) DH, (d) HD, (e) PF, (f) RMR, (g) CDR, and (h) overall evaluation.

(1) Evaluation Based on the Mean of Indicators

For the mean-based evaluation, Fig. 12(a)–(g) shows the overbreak risk classification cloud maps of each indicator, and Fig. 12(h) shows the comprehensive evaluation cloud map. AL, CSA, DH, HD, PF, and CDR are centered mainly in the medium-risk interval, whereas RMR is centered in the medium-low-risk interval. After comprehensive weighting, the overall evaluation cloud is distributed mainly in the medium-risk range, with part of the droplet cloud extending toward the medium-high-risk interval. This indicates that the mean-based comprehensive evaluation corresponds mostly to medium risk, with a tendency toward medium-high risk.

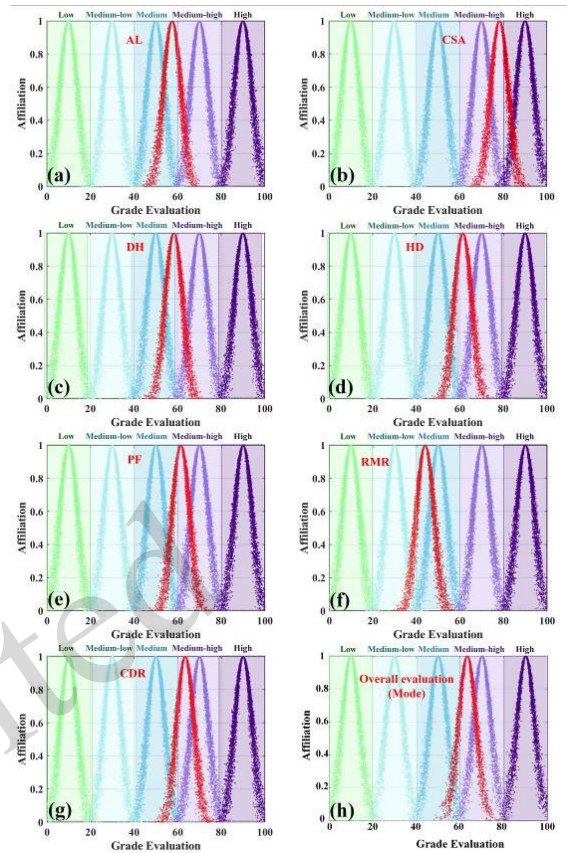


**Fig. 13** CE of overbreak based on cloud modeling using mode values: (a) AL, (b) CSA, (c) DH, (d) HD, (e) PF, (f) RMR, (g) CDR, and (h) overall evaluation.

(2) Evaluation Based on the Mode of Indicators

For the mode-based evaluation, Fig. 13(a)–(g) shows the overbreak risk classification cloud maps of each indicator, and Fig. 13(h) shows the corresponding comprehensive evaluation cloud map. AL, DH, and RMR are distributed mainly around the medium-risk level, whereas CSA, HD, PF, and CDR are concentrated mainly in the medium-high-risk interval. After comprehensive weighting, the overall mode-based evaluation cloud is located mainly in the medium-high-risk range, while part of the droplet cloud remains within the medium-risk interval. Therefore, the mode-based comprehensive evaluation can be classified as medium-high risk, with a transitional characteristic between the medium- and medium-high-risk levels.

(3) Comprehensive evaluation results based on cloud modeling

By comparing the comprehensive evaluation cloud maps derived from the mean and mode values, the overbreak risk of the HXT tunnel can be identified

as lying between the medium-risk and medium-high-risk levels. The mean-based result is classified mostly as medium risk but extends toward the medium-high-risk interval, whereas the mode-based result is classified mainly as medium-high risk. This interpretation is generally consistent with the actual OB-based assessment shown in Fig. 11. In particular, the mode-based comprehensive result agrees more closely with the actual assessment, while the mean-based result remains adjacent to it and reflects the same upward risk tendency.

These results indicate that the proposed cloud-model-based evaluation framework can reasonably capture the overall overbreak risk level as well as the boundary transition characteristics between adjacent grades. Rather than forcing the assessment into a rigid discrete class, the method provides a more interpretable description of uncertainty and grade tendency in practical engineering evaluation.

## 5 Forecast of overbreak area

After completing the cloud-model-based overbreak risk evaluation, the comprehensive evaluation scores obtained from the CE model were further used to predict the measured OB. Linear regression was performed using the evaluation score as the independent variable and the actual OB as the dependent variable. The fitted prediction equation is expressed as:

$$y = 7.47x + 22.27 \quad (9)$$

where  $x$  is the comprehensive evaluation score and  $y$  is the predicted OB.

The fitted regression relationship shows a clear positive correlation between the comprehensive evaluation score and the measured OB (Fig. 14). The model achieved an  $R^2$  value of 0.85. A scatter plot is presented together with the 95% confidence band and 95% prediction band. These results indicate that the comprehensive evaluation score can be used as an effective indicator for quantitative OB prediction, thereby linking qualitative risk evaluation with quantitative estimation.

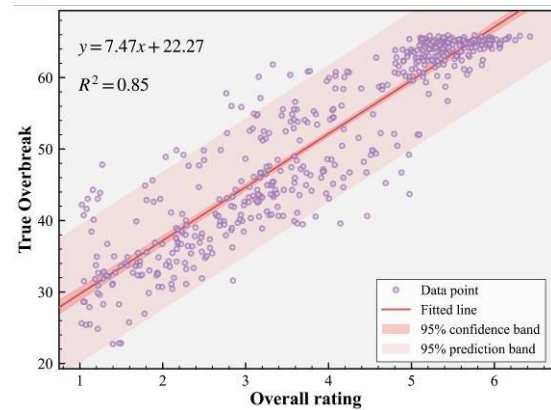


**Fig. 14** Fitted regression relationship between comprehensive evaluation score and measured overbreak area.

## 6 Conclusions

Given the adverse effects of overbreak on tunnel construction cost, schedule, and safety, this study proposed a cloud-model-based comprehensive evaluation and prediction framework by integrating fuzzy evaluation theory, multiple weighting methods, and ridge-regression-based objective weighting. A total of 523 records from the HXT tunnel were used, and seven indicators, namely RMR, CSA, CDR, PF, AL, HD, and DH, were selected to construct the overbreak evaluation system. The main conclusions are as follows:

(1) The proposed framework can support overbreak risk evaluation and prediction during tunnel construction. It can be used to identify the potential overbreak risk based on routinely obtainable geological and blasting parameters, thereby providing support for blasting design optimization and construction control.

(2) Among the tested objective weighting methods, the RR method achieved the best evaluation performance. By combining the best-performing objective weights with subjective weights, the final CE model achieved an evaluation accuracy of 85.28%, indicating good applicability to the HXT tunnel dataset.

(3) The cloud-model-based evaluation results show that the overbreak risk of the HXT tunnel lies between the medium-risk and medium-high-risk levels. The cloud model provides a visual representation of risk grades and their transitional characteristics, allowing both single-indicator and

comprehensive overbreak risk evaluation.

(4) The comprehensive evaluation score showed a clear linear relationship with the measured overbreak area. The fitted prediction model achieved an  $R^2$  value of 0.85, indicating that the evaluation score can be used as an effective indicator for quantitative overbreak area prediction.

In summary, the proposed framework provides an interpretable and practical tool for overbreak evaluation and prediction in tunnel blasting construction. However, the dataset used in this study was obtained from a single tunnel project. Therefore, the applicability of the model should be further validated using multi-project datasets under different geological and construction conditions.

### Acknowledgements

This research is partially supported by the National Natural Science Foundation of China (52474121), the Natural Science Foundation of Hunan Province (2026JJ20004), and the Scientific Research Foundation of Hunan Provincial Education Department (25A0011).

### Author contributions

Jian Zhou designed the research. Shibin Yao and Biao He processed the corresponding data. Shibin Yao wrote the first draft of the manuscript. Chuanqi Li helped to organize the manuscript. Jian Zhou revised and edited the final version.

### Conflict of interest

Shibin YAO, Jian ZHOU, Biao HE and Chuanqi LI declare that they have no conflict of interest.

### Data availability

The data that support the findings of this study are available from the corresponding author upon reasonable request.

### References

- Armaghani DJ, Asteris PG, 2021. A comparative study of ANN and ANFIS models for the prediction of cement-based mortar materials compressive strength. *Neural Computing and Applications*, 33:4501-4532. <https://doi.org/10.1007/s00521-020-05244-4>
- Asteris PG, Apostolopoulou M, Armaghani DJ, et al., 2020. On the metaheuristic models for the prediction of cement-metakaolin mortars compressive strength. *Metaheuristic Computing and Applications*, 1(1):63-99. <https://doi.org/10.12989/mca.2020.1.1.063>
- Asteris PG, Skentou AD, Bardhan A, et al., 2021. Predicting concrete compressive strength using hybrid ensembling of surrogate machine learning models. *Cement and Concrete Research*, 145:106449. <https://doi.org/10.1016/j.cemconres.2021.106449>
- Asteris PG, Tsavdaridis KD, Lemonis ME, et al., 2024. AI-powered GUI for prediction of axial compression capacity in concrete-filled steel tube columns. *Neural Computing and Applications*, 36:22429-22459. <https://doi.org/10.1007/s00521-024-10405-w>
- Barton N, 2002. Some new Q-value correlations to assist in site characterisation and tunnel design. *International Journal of Rock Mechanics and Mining Sciences*, 39(2):185-216. [https://doi.org/10.1016/S1365-1609\(02\)00011-4](https://doi.org/10.1016/S1365-1609(02)00011-4)
- Benzaamia A, Ghrici M, Rebouh R, et al., 2024. Predicting the shear strength of rectangular RC beams strengthened with externally-bonded FRP composites using constrained monotonic neural networks. *Engineering Structures*, 313:118192. <https://doi.org/10.1016/j.engstruct.2024.118192>
- Benzaamia A, Ghrici M, Rebouh R, et al., 2025. Prediction of chloride resistance level in concrete using optimized tree-based machine learning models. *Bulletin of Computational Intelligence*, 1(1):104-117. <https://doi.org/10.53941/bci.2025.100007>
- Bi S, Wang L, Li YR, et al., 2021. A comprehensive method for water environment assessment considering trends of water quality. *Advances in Civil Engineering*, 2021:5548113. <https://doi.org/10.1155/2021/5548113>
- Chen C, Yao S, Zhou J, 2025. Comparison of rock spalling evaluation in underground openings: uncertainty-based mathematical model and empirical method. *Deep Resources Engineering*, 2(2):100171. <https://doi.org/10.1016/j.deepr.2025.100171>
- Chen C, Zhou J, Zhou T, et al., 2021a. Evaluation of vertical shaft stability in underground mines: comparison of three weight methods with uncertainty theory. *Natural Hazards*, 109(2):1457-1479. <https://doi.org/10.1007/s11069-021-04885-5>
- Chen JH, Qiu WG, Zhao XW, et al., 2021b. Experimental and numerical investigation on overbreak control considering the influence of initial support in tunnels. *Tunnelling and Underground Space Technology*, 115:104017. <https://doi.org/10.1016/j.tust.2021.104017>
- Daraei A, Zare S, 2018. Prediction of overbreak depth in Ghalaje road tunnel using strength factor. *International Journal of Mining Science and Technology*, 28(4):679-684. <https://doi.org/10.1016/j.ijmst.2018.04.013>
- Dey K, Murthy VMSR, 2012. Prediction of blast-induced overbreak from uncontrolled burn-cut blasting in tunnels driven through medium rock class. *Tunnelling and Underground Space Technology*, 28:49-56. <https://doi.org/10.1016/j.tust.2011.09.004>
- Dong YP, Ren JG, Zhang ZF, et al., 2022. Development strategy of geology in next 5-10 years: trends and countermeasures. *Chinese Science Bulletin-Chinese*, 67(23):2708-2718 (in Chinese). <https://doi.org/10.1360/TB-2022-0194>

- Foderà GM, Voza A, Barovero G, et al., 2020. Factors influencing overbreak volumes in drill-and-blast tunnel excavation: a statistical analysis applied to the case study of the Brenner Base Tunnel-BBT. *Tunnelling and Underground Space Technology*, 105:103475. <https://doi.org/10.1016/j.tust.2020.103475>
- Friedman J, Hastie T, Tibshirani R, 2010. Regularization paths for generalized linear models via coordinate descent. *Journal of Statistical Software*, 33(1):1-22. <https://doi.org/10.18637/jss.v033.i01>
- Ganesan G, Mishra AK, 2021. Assessment of drilling inaccuracy and delineation of constructional and geological overbreak. *Tunnelling and Underground Space Technology*, 108:103730. <https://doi.org/10.1016/j.tust.2020.103730>
- Ghani S, Sapkota SC, Singh RK, et al., 2024. Modelling and validation of liquefaction potential index of fine-grained soils using ensemble learning paradigms. *Soil Dynamics and Earthquake Engineering*, 177:108399. <https://doi.org/10.1016/j.soildyn.2023.108399>
- Gong S, Yao SB, Xi FR, et al., 2022. A comparison of research methods to determine the sustainability of mineral resources in Henan Province based on cloud analysis. *Sustainability*, 14(23):15834. <https://doi.org/10.3390/su142315834>
- Gong S, Fan G, Chen J, et al., 2026a. Anisotropy of fracture behavior and 3D fracture surface morphology of Qinshui coal: laboratory experiments. *Theoretical and Applied Fracture Mechanics*, 105:105623. <https://doi.org/10.1016/j.tafmec.2026.105623>
- Gong S, Zhang H, Sun S, et al., 2026b. Effects of irregular holes defect on the entire dynamic progressive fracture process of SCT limestone in split Hopkinson pressure bar tests: laboratory experiments and FEM modeling. *Geomechanics and Geophysics for Geo-Energy and Geo-Resources*, 12:2. <https://doi.org/10.1007/s40948-025-01058-7>
- He B, Armaghani DJ, Lai SH, 2023. Assessment of tunnel blasting-induced overbreak: a novel metaheuristic-based random forest approach. *Tunnelling and Underground Space Technology*, 133:104979. <https://doi.org/10.1016/j.tust.2022.104979>
- He B, Armaghani DJ, Lai SH, et al., 2024a. A deep dive into tunnel blasting studies between 2000 and 2023: a systematic review. *Tunnelling and Underground Space Technology*, 147:105727. <https://doi.org/10.1016/j.tust.2024.105727>
- He B, Armaghani DJ, Lai SH, et al., 2024b. Applying data augmentation technique on blast-induced overbreak prediction: resolving the problem of data shortage and data imbalance. *Expert Systems with Applications*, 237:121616. <https://doi.org/10.1016/j.eswa.2023.121616>
- Hong ZX, Tao M, Cui XJ, et al., 2023a. Experimental and numerical studies of the blast-induced overbreak and underbreak in underground roadways. *Underground Space*, 8:61-79. <https://doi.org/10.1016/j.undsp.2022.04.007>
- Hong ZX, Tao M, Liu LL, et al., 2023b. An intelligent approach for predicting overbreak in underground blasting operation based on an optimized XGBoost model. *Engineering Applications of Artificial Intelligence*, 126:107097. <https://doi.org/10.1016/j.engappai.2023.107097>
- Hong ZX, Tao M, Zhao R, et al., 2023c. Investigation on overbreak and underbreak of pre-stressed tunnels under the impact of decoupled charge blasting. *International Journal of Impact Engineering*, 182:104784. <https://doi.org/10.1016/j.ijimpeng.2023.104784>
- Im H, Kurauchi T, Sato N, et al., 2025. Tunnel overbreak prediction: an integrated approach using 3D photogrammetry and machine learning. *Mining, Metallurgy & Exploration*, 42:1441-1457. <https://doi.org/10.1007/s42461-025-01278-1>
- Jang H, 2020. Tunnel overbreak management system using overbreak resistance factor. *Tunnel and Underground Space*, 30(1):63-75. <https://doi.org/10.7474/TUS.2020.30.1.063>
- Jang H, Kawamura Y, Shinji U, 2019. An empirical approach of overbreak resistance factor for tunnel blasting. *Tunnelling and Underground Space Technology*, 92:103060. <https://doi.org/10.1016/j.tust.2019.103060>
- Jang H, Topal E, 2013. Optimizing overbreak prediction based on geological parameters comparing multiple regression analysis and artificial neural network. *Tunnelling and Underground Space Technology*, 38:161-169. <https://doi.org/10.1016/j.tust.2013.06.003>
- Kim Y, Moon HK, 2013. Application of the guideline for overbreak control in granitic rock masses in Korean tunnels. *Tunnelling and Underground Space Technology*, 35:67-77. <https://doi.org/10.1016/j.tust.2012.11.008>
- Koopialipour M, Ghaleini EN, Haghighi M, et al., 2019. Overbreak prediction and optimization in tunnel using neural network and bee colony techniques. *Engineering with Computers*, 35(4):1191-1202. <https://doi.org/10.1007/s00366-018-0658-7>
- Krishnan AR, Kasim MM, Hamid R, et al., 2021. A modified CRITIC method to estimate the objective weights of decision criteria. *Symmetry-Basel*, 13(6):973. <https://doi.org/10.3390/sym13060973>
- Le TT, Skentou AD, Mamou A, et al., 2022. Correlating the unconfined compressive strength of rock with the compressional wave velocity, effective porosity, and Schmidt hammer rebound number using artificial neural networks. *Rock Mechanics and Rock Engineering*, 55:6805-6840. <https://doi.org/10.1007/s00603-022-02992-8>
- Lee SJ, Choi SO, Lee S, et al., 2016. Analysis of blasting overbreak using stereo photogrammetry in an underground mine. *Tunnel and Underground Space*,

- 26(5):348-362.  
<https://doi.org/10.7474/TUS.2016.26.5.348>
- Lei ZY, Guo JY, Zheng F, et al., 2022. Thyristor state evaluation method based on kernel principal component analysis. *IEEE Access*, 10:29992-30004.  
<https://doi.org/10.1109/ACCESS.2022.3159711>
- Li DY, Liu CY, Gan WY, 2009. A new cognitive model: cloud model. *International Journal of Intelligent Systems*, 24(3):357-375.  
<https://doi.org/10.1002/int.20340>
- Li SC, Wu J, 2019. A multi-factor comprehensive risk assessment method of karst tunnels and its engineering application. *Bulletin of Engineering Geology and the Environment*, 78(3):1761-1776.  
<https://doi.org/10.1007/s10064-017-1214-1>
- Li ZQ, Li Z, Huang WW, et al., 2023. Study on influence of key blasthole parameters on tunnel overbreak. *Underground Space*, 9:76-90.  
<https://doi.org/10.1016/j.undsp.2022.07.001>
- Liang LW, Wang ZB, Li JX, 2019. The effect of urbanization on environmental pollution in rapidly developing urban agglomerations. *Journal of Cleaner Production*, 237:117649.  
<https://doi.org/10.1016/j.jclepro.2019.117649>
- Liu WJ, An YL, Zhou J, 2024. Study on potential collapse of deep-buried tunnel induced by local overbreak obeying Hoek-Brown failure criterion. *Tunnelling and Underground Space Technology*, 145:105586.  
<https://doi.org/10.1016/j.tust.2024.105586>
- Liu YS, Li A, Zhang H, et al., 2023. Minimization of overbreak in different tunnel sections through predictive modeling and optimization of blasting parameters. *Frontiers in Ecology and Evolution*, 11:1255384.  
<https://doi.org/10.3389/fevo.2023.1255384>
- Mandal SK, Singh MM, 2009. Evaluating extent and causes of overbreak in tunnels. *Tunnelling and Underground Space Technology*, 24(1):22-36.  
<https://doi.org/10.1016/j.tust.2008.01.007>
- Mottahedi A, Sereshki F, Ataei M, 2018. Development of overbreak prediction models in drill and blast tunneling using soft computing methods. *Engineering with Computers*, 34(1):45-58.  
<https://doi.org/10.1007/s00366-017-0520-3>
- Nakagawa S, Schielzeth H, 2013. A general and simple method for obtaining  $R^2$  from generalized linear mixed-effects models. *Methods in Ecology and Evolution*, 4(2):133-142.  
<https://doi.org/10.1111/j.2041-210x.2012.00261.x>
- Sarir P, Chen J, Asteris PG, et al., 2021. Developing GEP tree-based, neuro-swarm, and whale optimization models for evaluation of bearing capacity of concrete-filled steel tube columns. *Engineering with Computers*, 37(1):1-19.  
<https://doi.org/10.1007/s00366-019-00808-y>
- Sun SR, Liu JM, Wei JH, 2013. Predictions of overbreak blocks in tunnels based on the wavelet neural network method and the geological statistics theory. *Mathematical Problems in Engineering*, 2013:706491.  
<https://doi.org/10.1155/2013/706491>
- Taheri S, Topal E, Nguyen H, et al., 2025. Predicting overbreak and underbreak in underground longhole stoping using meta-soft computing models. *Tunnelling and Underground Space Technology*, 164:106852.  
<https://doi.org/10.1016/j.tust.2025.106852>
- Torres VFN, Da Gama CD, Sotomayor JMG, 2023. Post-work inspection for overbreak in tunnels: a case study application to the Alqueva hydroelectric plant. *Geomechanics and Geoengineering*, 18(1):80-89.  
<https://doi.org/10.1080/17486025.2021.2012075>
- Verma HK, Samadhiya NK, Singh M, et al., 2018. Blast induced rock mass damage around tunnels. *Tunnelling and Underground Space Technology*, 71:149-158.  
<https://doi.org/10.1016/j.tust.2017.08.019>
- Xiao FY, Cao ZH, Lin CT, 2023. A complex weighted discounting multisource information fusion with its application in pattern classification. *IEEE Transactions on Knowledge and Data Engineering*, 35(8):7609-7623.  
<https://doi.org/10.1109/TKDE.2022.3206871>
- Yang XY, Wang H, Gu YQ, et al., 2024. Comprehensive assessment and empirical research on green and low-carbon technologies in the steel industry. *Processes*, 12(2):397.  
<https://doi.org/10.3390/pr12020397>
- Yao S, Li X, Zhou J, et al., 2025a. Graded evaluation and optimal scheme selection of mine rock diggability based on the multidimensional cloud model. *Machines*, 13(11):1019.  
<https://doi.org/10.3390/machines13111019>
- Yao S, Zhou J, Khandelwal M, et al., 2025b. Intelligent decision framework for booster fan optimization in underground coal mines: hybrid spherical fuzzy-cloud model approach enhancing ventilation safety and operational efficiency. *Machines*, 13(5):367.  
<https://doi.org/10.3390/machines13050367>
- Zeng J, Roussis PC, Mohammed AS, et al., 2021. Prediction of peak particle velocity caused by blasting through the combinations of Boosted-CHAID and SVM models with various kernels. *Applied Sciences*, 11(8):3705.  
<https://doi.org/10.3390/app11083705>
- Zhang YW, Zhang YD, Song ZP, et al., 2024. A LFPP-FAHP based evaluation model of blasting scheme for tunnel undercrossing existing buildings. *Tunnelling and Underground Space Technology*, 153:105937.  
<https://doi.org/10.1016/j.tust.2024.105937>
- Zhao J, Nguyen H, Nguyen-Thoi T, et al., 2022. Improved Levenberg-Marquardt backpropagation neural network by particle swarm and whale optimization algorithms to predict the deflection of RC beams. *Engineering with Computers*, 38(Suppl 5):3847-3869.  
<https://doi.org/10.1007/s00366-020-01267-6>
- Zhao Q, Du YX, Zhang TT, et al., 2021. Resilience index system and comprehensive assessment method for distribution network considering multi-energy

- coordination. *International Journal of Electrical Power & Energy Systems*, 133:107211.  
<https://doi.org/10.1016/j.ijepes.2021.107211>
- Zhao YG, Zhong WQ, 2009. A quality evaluation method for existing carbonated reinforced concrete members. *Structure and Infrastructure Engineering*, 5(2):137-144.  
<https://doi.org/10.1080/15732470600956849>
- Zhou J, Asteris PG, Armaghani DJ, et al., 2020. Prediction of ground vibration induced by blasting operations through the use of the Bayesian Network and random forest models. *Soil Dynamics and Earthquake Engineering*, 139:106390.  
<https://doi.org/10.1016/j.soildyn.2020.106390>
- Zhou J, Chen C, Armaghani DJ, et al., 2022a. Developing a hybrid model of information entropy and unascertained measurement theory for evaluation of the excavatability in rock mass. *Engineering with Computers*, 38:247-270.  
<https://doi.org/10.1007/s00366-020-01053-4>
- Zhou J, Chen C, Wei C, et al., 2022b. An improved connection cloud model of an updated database: a multicriteria uncertainty model for coal burst liability evaluation. *Natural Resources Research*, 31(3):1687-1704.  
<https://doi.org/10.1007/s11053-022-10042-x>
- Zhou J, Chen C, Khandelwal M, et al., 2022c. Novel approach to evaluate rock mass fragmentation in block caving using unascertained measurement model and information entropy with flexible credible identification criterion. *Engineering with Computers*, 38(Suppl 5):3789-3809.  
<https://doi.org/10.1007/s00366-020-01230-5>
- Zhou J, Chen C, Du K, et al., 2022d. A new hybrid model of information entropy and unascertained measurement with different membership functions for evaluating distressability in burst-prone underground mines. *Engineering with Computers*, 38:381-399.  
<https://doi.org/10.1007/s00366-020-01151-3>
- Zhou J, Yao S, Monjezi M, et al., 2026. Comprehensive evaluation and prediction model for blasting fragmentation in mining based on fuzzy theory and multiple weighting methods. *Natural Resources Research*, 35:653-677.  
<https://doi.org/10.1007/s11053-025-10583-x>

## Electronic supplementary materials

Sections S1-S3, Figs. S1 and S4, Eqs. S1-S18

## 中文概要

**题目:** 基于云模型与模糊评价理论的隧道超挖综合评价与预测方法

**作者:** 姚世斌<sup>1</sup>, 周健<sup>1</sup>, 何彪<sup>2</sup>, 李传奇<sup>1</sup>

**机构:** <sup>1</sup>中南大学, 资源与安全工程学院, 中国长沙, 410083; <sup>2</sup>科克大学, 土木、结构与环境工程系, 爱尔兰科克

**目的:** 钻爆法隧道施工过程中, 地质条件、钻孔精度、装药结构和爆破参数等因素共同影响超挖形成, 导致实际开挖轮廓超出设计边界, 进而增加出渣、回填和支护成本, 并可能影响围岩稳定性与施工安全。本文旨在针对隧道超挖评价中指标多源、边界模糊和等级过渡不确定等问题, 建立一种融合云模型、模糊评价理论和主客观组合赋权的综合评价与预测方法, 实现隧道超挖风险等级识别、等级过渡特征表征和超挖面积定量预测, 为钻爆法隧道施工中的超挖控制和爆破参数优化提供参考。

**创新点:** 1. 建立了考虑地质条件与爆破参数的隧道超挖多指标评价体系; 2. 对比多种客观赋权方法, 并将最优客观权重与专家主观权重融合, 构建综合评价模型; 3. 通过云模型实现超挖风险等级及等级过渡的可视化表达; 4. 建立了综合评价得分与超挖面积之间的预测关系。

**方法:** 1. 基于 HXT 隧道 523 组现场数据, 选取围岩质量评分、断面面积、装药深度比、单位耗药量、循环进尺、炮孔密度和炮孔深度等 7 个指标, 建立隧道超挖评价指标体系 (图 4); 2. 采用多种客观赋权方法和专家主观赋权方法计算指标权重, 并通过评价准确率筛选最优客观赋权结果, 进一步构建主客观融合的综合评价模型 (表 1)。利用云模型生成超挖风险等级云图, 对实测超挖面积及综合评价结果进行可视化分析, 表征超挖风险等级及相邻等级过渡特征 (图 10-13); 以综合评价得分为自变量、实测超挖面积为因变量建立线性回归模型, 得到超挖面积预测公式 (公式(9)), 并验证综合评价得分对超挖面积的预测能力 (图 14)。

**结论:** 1. 岭回归赋权方法在客观赋权方法中表现最优, 评价准确率为 83.75%; 融合专家主观权重后, 综合评价模型的评价准确率提高至 85.28%; 2. 云模型评价结果表明, HXT 隧道整体超挖风险位于中风险至中高风险之间, 且具有相邻等级过渡特征; 3. 基于指标众数的综合评价结果与实测超挖面积评价结果更为接近, 说明所建模型能够较好反映隧道超挖风险状态; 4. 综合评价得分与实测超挖面积之间具有明显线性关系, 预测模型的  $R^2$  为 0.85, 可用于超挖面积定量预测。

**关键词:** 隧道超挖; 风险评价; 云模型; 模糊评价; 岭回归; 综合评价模型